Original article

Structural deformation of shale pores in the fold-thrust belt: The Wufeng-Longmaxi shale in the Anchang Syncline of Central Yangtze Block

Xiaochen Guo[1], Rui Liu[1]*, Shang Xu[2]*, Bing Feng[3], Tao Wen[4], Tingshan Zhang[1]

[1]*School of Geoscience and Technology, Southwest Petroleum University, Chengdu 610500, P. R. China*

[2]*School of Geosciences, China University of Petroleum (East China), Qingdao 266580, P. R. China*

[3]*Guizhou Shale Gas Exploration and Development Co. LTD, Guiyang 550001, P. R. China*

[4]*Department of Earth and Environmental Sciences, Syracuse University, Syracuse, NY 13244, USA*

Abstract:
The gas-rich Wufeng-Longmaxi shale has been intensely deformed within the fold-thrust belt of the Yangtze Block. To better understand the impact of structural deformation on the shale pore system, this paper systematically investigated the matrix components, porosity and pore structures in core samples from the Wufeng-Longmaxi shale, newly collected from various structural domains in the first commercial shale gas field of the Central Yangtze Block, the Anchang Syncline. The shale porosity generally showed a positive relationship with total organic carbon content. Nevertheless, even at a constant total organic carbon content, the shale porosity decreased from the syncline limb to the syncline hinge zone and with a decreasing interlimb angle in the syncline hinge zone, which aligned with the structural deformation strain during folding. The artificial axial compression of shale samples also confirmed that the decrease in shale porosity was stronger at an elevated axial compression stress and was relatively higher in samples with higher total organic carbon content. The organic pore size decreased with higher structural deformation strain, but the aspect ratio of the pore shape increased. Even quartz failed to resist the effective stress under the intensive structural deformation, changing the correlation between porosity and quartz from positive to negative. In contrast, pore spaces generated by the slipping between clay flakes under intensive deformation accounted for a positive relationship between clay content and bulk porosity. Considering the shale porosity reduction caused by the intensive structural deformation of shale pores, the Wufeng-Longmaxi shale, that is rich in fracture networks between roof and floor layers, may still be an excellent exploration target in the fold-thrust belt of the Yangtze Block.

1. Introduction

Characterizing pore structures in shale at the submicron to nanometer scales by scanning electron microscopy (SEM) has revealed that organic-rich shale is a source as well as a reservoir of hydrocarbons that are generated by organic matter within the shale via thermogenic or biogenic processes (Loucks et al., 2009). In the last decade, this discovery greatly promoted the global exploration and exploitation of hydrocarbons in unconventional shale reservoirs (McGlade et

al., 2013). Nevertheless, a comprehensive understanding of multiscale pore development in organic-rich shales is still lacking (Katz and Arango, 2018; Cai et al., 2022; Xu et al., 2020).

Previous viewpoints of shale pore evolution were influenced by stress-controlled mechanical deformation or thermal-powered chemical diagenesis (Gao et al., 2020; Li et al., 2020; Liu et al., 2020a; Sheng et al., 2020). The direct imaging of micro- to nanoscale pores in organic matter (Loucks et al.,

2009; Curtis et al., 2010), as well as the linear relationship between total organic carbon (TOC) content and bulk porosity (Chalmers and Bustin, 2007; Jarvie, 2012) in North American shales, suggested the dominance of organic porosity in shale pore systems. Subsequently, natural cores of organic-rich shales with various thermal maturities were analyzed (e.g., the Posidonia shale (Bernard et al., 2012a; Mathia et al., 2016; Han et al., 2017), Barnett shale (Bernard et al., 2012b), Woodford shale (Curtis et al., 2012; Lohr et al., 2015), New Albany shale (Mastalerz et al., 2013; Liu et al., 2017a), Eagle Ford shale (Pommer and Milliken, 2015), and Haynesville and Bossier shales (Klaver et al., 2015)), and artificial heating experiments were performed on low-maturity shales (e.g., the Woodford shale (Hu et al., 2015), Yanchang Formation (Chang 7 Member) (Sun et al., 2015), Boquillas Formation (Ko et al., 2016), and Barnett shale (Ko et al., 2018)). The above studies served to characterize the organic pore generation process, which is powered by the thermal cracking of organic matter. In general, there is no monotonic correlation between thermal maturation and organic pore generation (Loucks et al., 2012). Massive organic pores in shale appear to be rare within the oil window as a result of oil or bitumen occlusion (Lohr et al., 2015; Han et al., 2017), or kerogen or clay swelling (Mathia et al., 2016), whereas they are stimulated by primary or secondary gas generation at elevated levels of thermal maturity (Bernard et al., 2012a; Curtis et al., 2012; Mastalerz et al., 2013; Pommer and Milliken, 2015; Ko et al., 2016; Chen et al., 2021). Even at the same TOC content and thermal maturity level, organic porosity can be quite variable because of differences in expulsion efficiency (Liu et al., 2017b) and maceral type (Curtis et al., 2012; Loucks et al., 2012; Lohr et al., 2015), which can alter the hydrocarbon generation potential.

Nevertheless, the thermal maturity level roughly positively correlates with burial depth. With increasing burial depth and sedimentary overburden, the porosity of sedimentary rocks is generally decreased due to pore collapse (Athy, 1930; Bjørlykke, 2014). Lohr et al. (2015) pointed out that the reducing effect of compaction caused by increased plasticity at high temperatures on the organic porosity within the matured Woodford shale cannot be ignored. A similar porosity loss caused by compaction in the oil window was also reported in the Kimmeridge mudstones (Fishman et al., 2012) and Posidonia shale (Mathia et al., 2016). Milliken et al. (2013) reported that the bulk porosity of both matured (at vitrinite reflectance (R_o) of 1.0%) and highly matured (at R_o of 2.1%) Marcellus shale positively correlates with TOC content when TOC $<$ 5.6 wt.%, but it becomes independent of TOC content when TOC $>$ 5.6 wt.%. One possible mechanism of this complex relationship is that pore collapse is facilitated by a higher content of organic matter, which has a relatively lower ability to preserve pores after compaction (Milliken et al., 2013). Wang (2020) also provided some insights into the nature of organic pore deformation in the highly matured Longmaxi shale (with bitumen reflectance ranges from 3.0% to 4.0%).

Apart from vertical compaction driven by overburden stress, the compaction (or deformation) of the shale pore system can also be prompted by lateral tectonic compression (Evans et al., 1989; Screaton et al., 2002). Outcrop samples of the Lujiaping shale (Lower Cambrian) and Longmaxi shale obtained from compression anticlines (meters in width) indicated that ductile folding destroyed macropores, but resulted in massive micro- and mesopores (Zhu et al., 2018, 2019; Ma et al., 2020; Shi et al., 2021; Xiang et al., 2021). Meanwhile, industrial drilling cores of the Wufeng-Longmaxi shale collected from compression anticlines (scale of tens of kilometers) of the Fuling (Liu et al., 2020a; Gou et al., 2021) and Changning (Liu et al., 2020b) areas indicated that the deformation of a shale pore system, particularly organic pores, accounted for abnormally low porosity and high TOC content in some particular structural domains; shale porosity was decreased to a greater extent in the core and forelimb areas of thin-skinned and basement-involved anticlines, respectively, than others. A similar variation in pore structural damage in the structural domains was identified in lacustrine shale reservoirs (Emuerhe and Ershierzhan Formations) of the Mohe Basin (Hou et al., 2021).

As mentioned above, the Wufeng-Longmaxi shale in the Upper Yangtze Block, which has suffered multistage tectonic compressions (Hao and Zou, 2013; Liu et al., 2019; Xu et al., 2019), recently became an ideal natural laboratory to analyze the impact of tectonic compaction (or deformation) on shale pore systems. However, relevant works have primarily focused on the anticline structures and rarely discussed syncline formations (Gu et al., 2021). In this study, an investigation of tectonic compaction was carried out on cores from the Wufeng-Longmaxi shale that were recently drilled from the Anchang Syncline (Fig. 1), which is located in the Central Yangtze Block outside the Sichuan Basin. The Anchang Syncline was the first commercial shale gas field in Guizhou Province of China and was developed by a local energy company.

2. Geological setting

The Yangtze Block of South China is separated from the Songpan Block by the Longmenshan Fault in the west, from the Cathaysian Block by the Jiangnan-Xuefeng Orogen in the east, and from the North China Block by the Qinling-Dabie Fault in the north (Fig. 1(a)). Starting in the Neoproterozoic, the subduction of the Cathaysian Block beneath the Yangtze Block resulted in the uplift of the Jiangnan-Xuefeng Orogen (Dong et al., 2015, 2020; Zhang et al., 2021). Subsequently, the Yangtze Block became an active continental margin and received shallow- to deepwater siliciclastic and carbonate depositions in platform-to-slope settings during the Paleozoic. Thereafter, the concurrence of sea-level changes, glaciations, mass extinctions, and oceanic anoxia during the Late Ordovician-Early Silurian (Melchin et al., 2013; Zou et al., 2018) contributed to the deposition and preservation of massive organic matters in the Wufeng-Longmaxi shale (Fig. 1(a)). During the Triassic, the Yangtze Block converged with the North China Block and Indochina Block in the north and south, respectively. Throughout the Late Jurassic-Early Cretaceous (also called the Yanshanian period), the orogenic process of the Jiangnan-Xuefeng Orogen generated a NE-
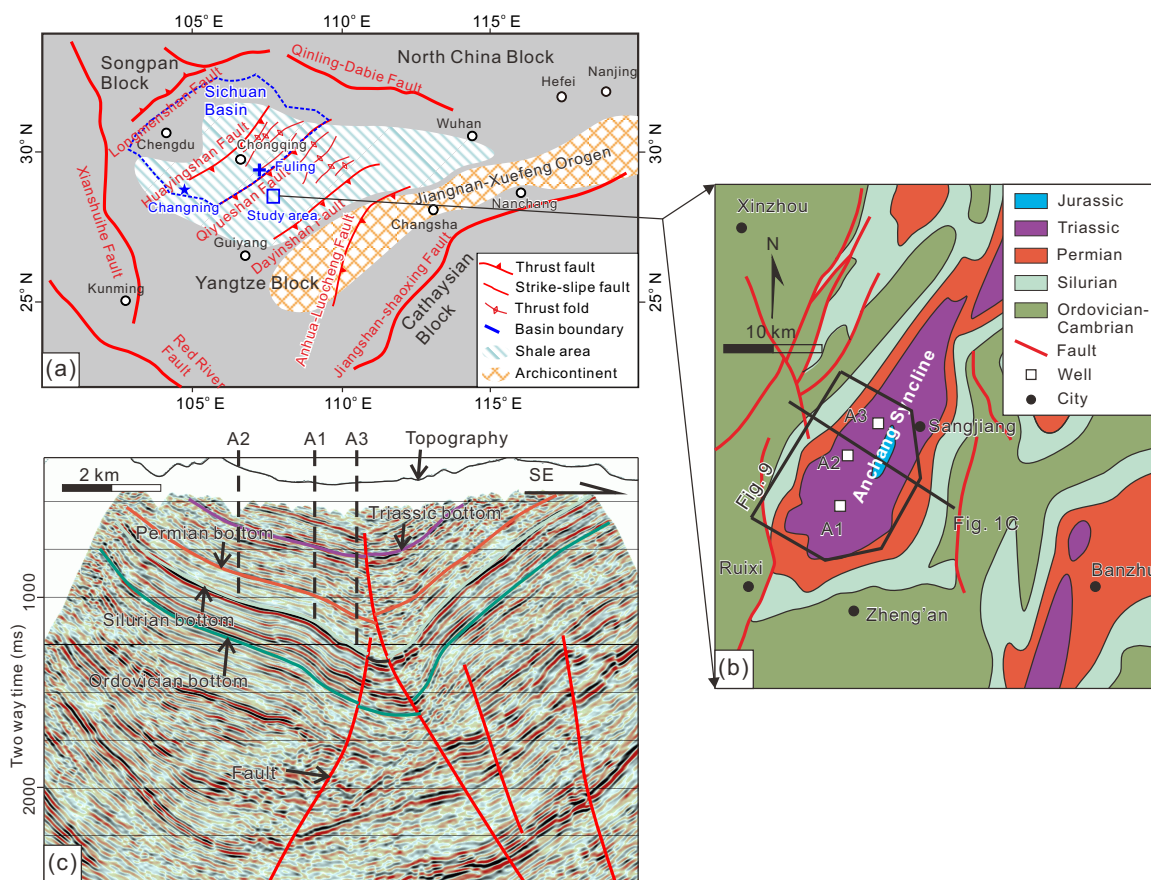
Fig. 1. Tectonic settings of (a) the Yangzte Block and (b) the Anchang Syncline, (c) a seismic reflection profile of the Anchang Syncline, with the profile location indicated in Fig. 1(b). Locations of sampling wells are also indicated..

striking fold-thrust belt with a width of hundreds of kilometers in the Central and Eastern Yangtze Block. In the Cenozoic (also called the Himalayan period), the eastward extrusion of the Tibetan Plateau collided with the Yangtze Block along the Longmenshan fault belt.

The Anchang Syncline, located in the northern Zheng'an City of Guizhou Provence and having an area of > 200 km², shows an outline narrowing to the north (Fig. 1(b)). It tectonically belongs to the fold-thrust belt of the Central Yangtze Block and was formed by compression and ex-humation during the Late Jurassic-Early Cretaceous. The first shale-gas well in the Anchang Syncline was drilled in 2015, revealing a gas content of up to 6.49 m³/t and gas reserves of 50 billion m³ in the Wufeng-Longmaxi shale (Zhai et al., 2017). The Wufeng-Longmaxi shale of the Anchang Syncline is characterized by black color, is rich in graptolite, has 16-25 m thickness and possesses 1.08-4.73 wt.% of TOC content (with an average value of 2.65 wt.%) (Zhai et al., 2017). The thermal maturity level of Wufeng-Longmaxi shale was estimated to be 1.92%-2.19% R_o, indicating a deepest burial depth of > 5000 m before exhumation (Zhai et al., 2017; Feng et al., 2018). Nevertheless, the current burial depth of Wufeng-Longmaxi shale ranges from the ground surface (outcrop) to approximately 2,000-3,000 m (Fig. 1(c)) at the center of the Anchang Syncline.

3. Samples and methods

Cores from the Wufeng-Longmaxi shale were collected from three newly drilled wells in the Anchang Syncline: (A1) at a depth of 2,330-2,350 m, (A2) at a depth of 1,955-1,975 m, and (A3) at a depth of 2,470-2,490 m (Fig. 2). As shown in Fig. 1(b), the interlimb angle of the Anchang Syncline generally decreases from south to north. The wells of A1 and A3 were chosen for their difference in interlimb angles in the syncline hinge zone, whereas A2 was viewed as a proxy for the syncline limb.

3.1 Total organic carbon

A total of 59 crushed samples (22, 20 and 17 samples from wells A1, A2 and A3, respectively) were pretreated with 5% hydrochloric acid to eliminate the effect of carbonates, and their TOC contents were determined by burning in a LECO CS-200 elemental analyzer.

3.2 X-ray diffraction

The bulk mineralogical composition of 41 samples (21, 8 and 12 samples from wells A1, A2 and A3, respectively) was examined by X-ray diffraction (XRD). Powdered samples (∼100 mesh) were analyzed by a Bruker D8 X-ray diffrac-tometer (Cu-Ka radiation, 40 kV, and 30 mA). Stepped scann-
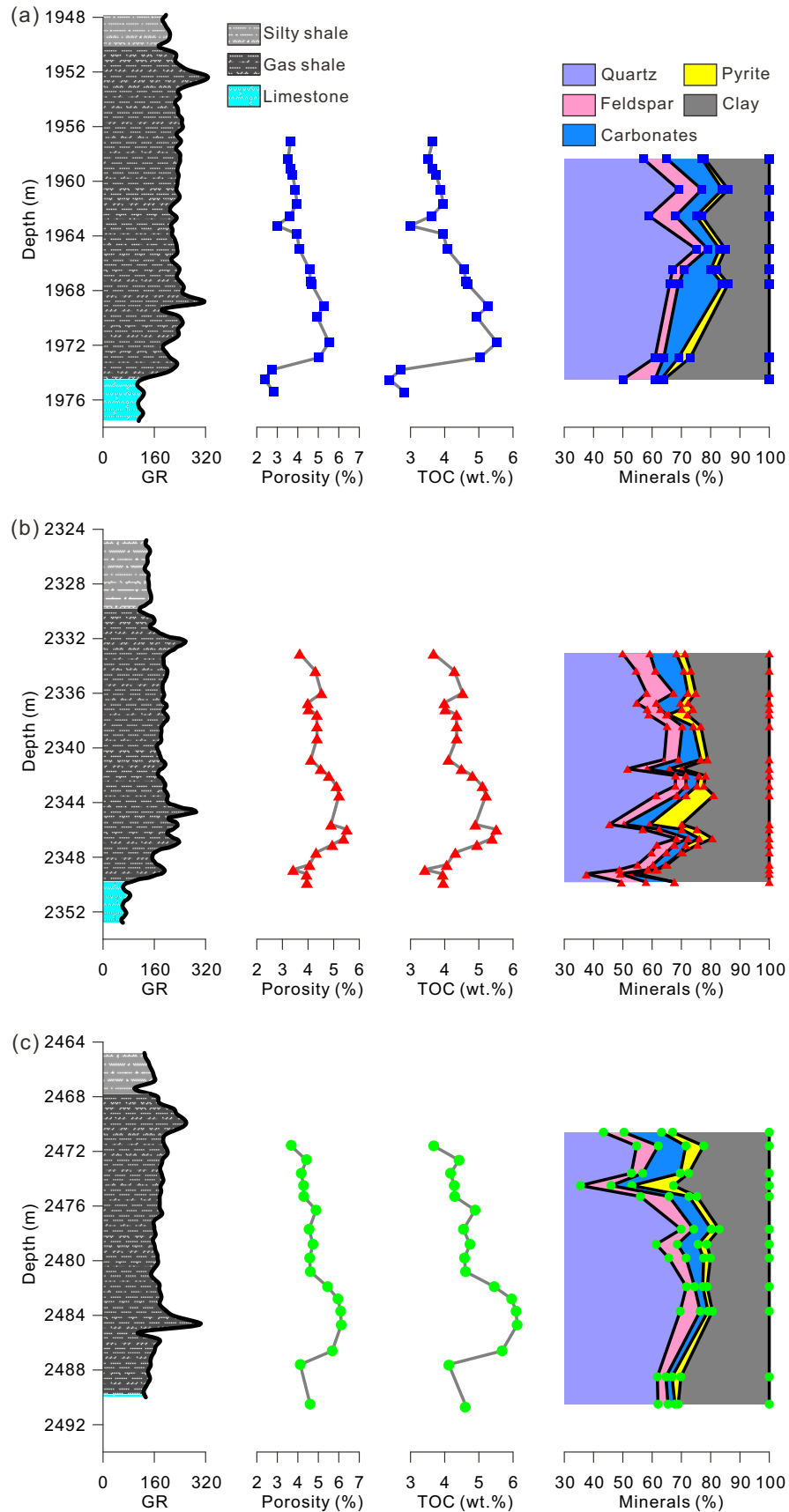
Fig. 2. Data profiles of wells (a) A2, (b) A1 and (c) A3 in the Anchang Syncline. GR is the natural gamma-ray logging (API), TOC is the total organic carbon, and Carbonates include dolomite and calcite.
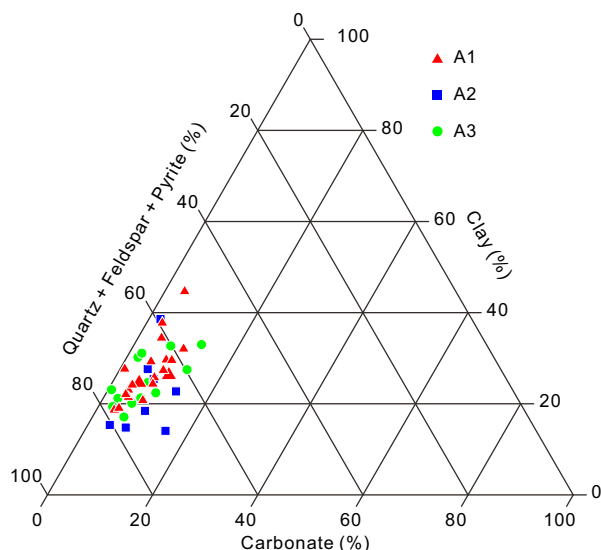
Fig. 3. Ternary diagram of mineral composition in the Wufeng-Longmaxi shale samples of the Anchang Syncline.

ing measurements were operated within the range of 3 °-85 ° (2θ) at a rate of 4 °/min. The XRD patterns were interpreted by HighscorePlus software for quantitative mineral phase analyses.

3.3 Helium porosimetry

Porosity was estimated using helium porosimetry based on Boyle's Law. A total of 55 samples (21, 17 and 17 samples from wells A1, A2 and A3, respectively), prepared following the instructions of Fraser-Harris et al. (2020), were dried at 105 °C until weight constancy before the measurement of grain densities. The bulk density of cylindrical plugs was measured by a caliper, and the bulk density of rock fragments was determined utilizing the mercury immersion technique. Porosity was considered according to a combination of bulk and grain densities.

Cylindrical plugs from well A1 with diameters of 25.4 mm and lengths ranging from 25 to 40 mm (without visible cracks), drilled parallel to the bedding, were placed in the uniaxial (or triaxial) chamber of a PoroPDP-200 full-automatic porosimeter for the determination of porosity and pore volume at an axial compression of 20 and 30 MPa with helium.

3.4 Scanning electron microscopy

The polished surface of rock fragments was ion-milled utilizing a broad argon ion beam at a relatively low angle. High-resolution imaging of the polished surfaces was achieved by employing a Zeiss Sigma 300 FE-SEM (Field-Emission Scanning Electron Microscope).

4. Results

4.1 Matrix components

Despite that mineral composition varies vertically with burial depth because of the sea-level fluctuation during deposition (Fig. 2), the Wufeng-Longmaxi shale samples in the three drilled wells of the Anchang Syncline showed similar

XRD mineralogy (Fig. 3), which mainly consisted of feldspar and quartz, followed by clay minerals varying from 14.0% to 38.1% (with an average of 25.6%) and carbonate minerals varying from 2.0% to 12.8% (with an average of 6.3%). The quartz content was between 37.5%-75.0% (with an average of 58.6%) and it negatively correlated with clay content (Fig. 4(a)).

The Wufeng-Longmaxi shale samples had a TOC content of 3.42-5.21 wt.% (with an average of 4.44 wt.%) in well A1, 2.38-5.53 wt.% (with an average of 4.00 wt.%) in well A2, and 3.68-6.12 wt.% (with an average of 4.84 wt.%) in well A3. The TOC content related positively and negatively with quartz and clay contents, respectively (Figs. 4(b) and 4(c)).

4.2 Shale porosity

The Wufeng-Longmaxi shale samples showed a porosity of 2.67%-6.17% (with an average of 3.74%) in well A1, 2.99%-6.37% (with an average of 4.37%) in well A2, and 1.38%-6.52% (with an average of 3.08%) in well A3. Porosity positively changed with TOC content for samples from all three wells (Fig. 5(a)). Nevertheless, with the same TOC content, shale porosity was commonly the highest in samples obtained from well A2 and the lowest in those from well A3 (Fig. 5(a)). The shale porosity of samples obtained from well A3 positively changed with the clay content (Fig. 5(b)) but were negatively related to the quartz content (Fig. 5(c)). Samples from well A2 showed a negative interrelation between porosity and clay content (Fig. 5(b)) but a positive interrelation between porosity and quartz content (Fig. 5(c)). Porosity generally positively correlated with pyrite content in samples from all wells (Fig. 5(d)). A monotonic linear correlation between porosity and relatively soluble minerals (e.g., feldspar and carbonates) appeared occasionally (Figs. 5(e) and 5(f)).

The shale porosity of samples from well A1 distinctly decreased after uniaxial compression (Fig. 6(a)). The absolute magnitude of porosity change (where a negative sign indicates the porosity reduction) increased with uniaxial compression stress and was generally higher in samples with higher TOC content (Fig. 6(b)). The change in porosity after compression relative to the initial porosity was generally higher with stronger compression, but was negatively related to the TOC content (Fig. 6(c)).

4.3 Pore structures

The FE-SEM observations of the Wufeng-Longmaxi shale samples collected from the three wells in the Anchang Syncline revealed various micro- to nanometer-sized pores, including those in organic matter (organic pores) (Fig. 7(a)) and in the framework minerals (Figs. 7(b)-7(e)).

4.3.1 Mineral-associated pores

Intergranular pores commonly appeared to be associated with authigenic microcrystalline quartz and pyrite framboids (Fig. 7(c)) and were widely occluded with organic matter. Some of the pyrite framboids were deformed and elongated by compaction. Intragranular pores were well developed along with cleavage plates of clay minerals and were linear in
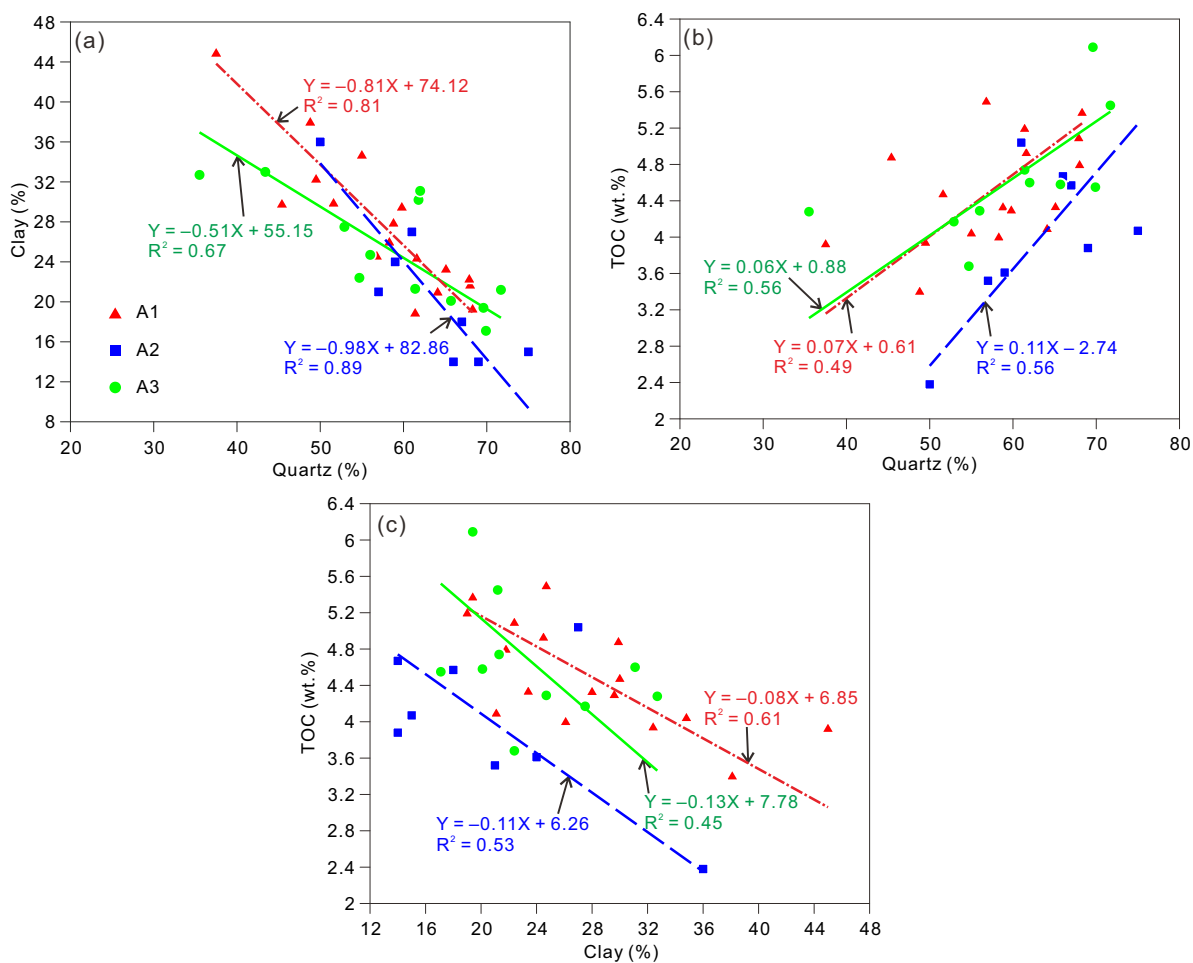
Fig. 4. Crossplots of (a) quartz with clay contents, (b) quartz with total organic carbon (TOC) contents and (c) clay and TOC contents for the Wufeng-Longmaxi shale samples collected from three wells in the Anchang Syncline.

shape, with lengths reaching several micrometers, but with narrow widths of up to hundreds of nanometers (Figs. 7(d) and 7(e)). The clay flakes were deformed and split by compaction stresses (Figs. 7(d) and 7(e)), and cleavage-associated pores were generated by the bending of clay flakes. Intragranular pores generated by dissolution were commonly observed in feldspar and carbonate grains (Fig. 7(f)).

4.3.2 Organic pores

In this study, organic pores were widely identified in the pore system of the Wufeng-Longmaxi shale samples. Most of the organic pores in the FE-SEM observations were macropores (> 50 nm in diameter) in samples obtained from well A2 (Figs. 8(a)-8(c)), whereas mesopores (2-50 nm in diameter) dominated in samples obtained from well A3. Both macropores and mesopores commonly appeared in the samples of well A1. The pore shapes were generally characterized by a typical round morphology in the samples of well A2 (Figs. 8(a)-8(c)), while they exhibited polygonal, elongated and slit morphologies in samples from wells A1 and A3 (Figs. 8(d)-8(i)).

5. Discussion

5.1 Controlling factors of TOC-porosity correlation

Organic matter is commonly considered as the primary host of pore systems in organic-rich shale, which results in a positive relationship between porosity and TOC content (Chalmers and Bustin, 2007; Jarvie, 2012). Not only we discovered massive pores in the organic matter (Fig. 8) in the Wufeng-Longmaxi shale samples obtained from the three wells in the Anchang Syncline, but also observed positive relationships between TOC and porosity (Fig. 5(a)). However, both the size and shape of organic pores as well as the coefficient of the TOC-porosity correlation varied spatially between the three wells, implying that certain factors altered the relationship between porosity and TOC content in the Wufeng-Longmaxi shale of the Anchang Syncline.

5.1.1 Thermal evolution of organic matter

As mentioned in the Introduction section, the potential for organic pore generation through thermal cracking varies with the thermal level and maceral type, affecting the TOC-
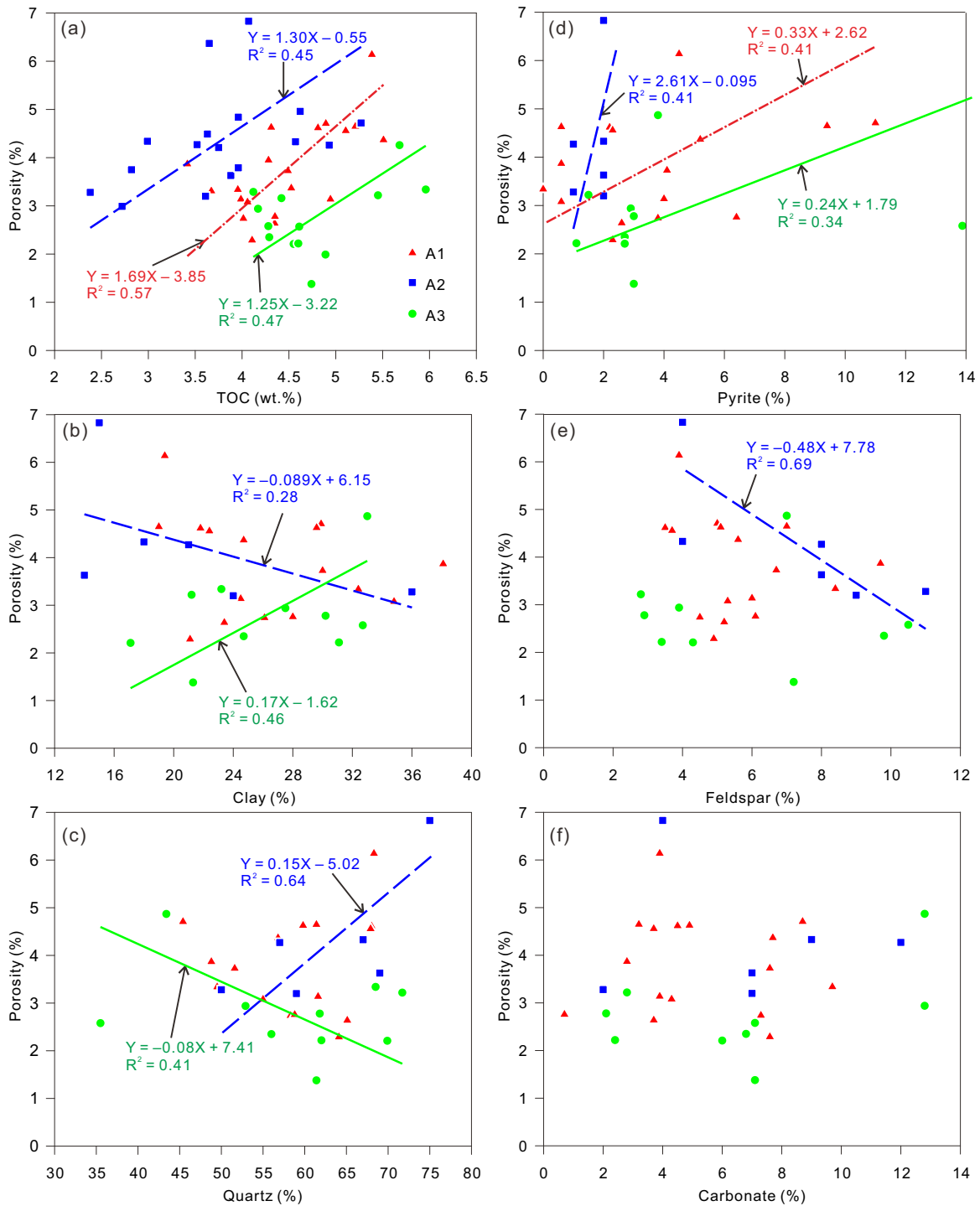
Fig. 5. Crossplots of porosity with (a) TOC, (b) clay, (c) quartz, (d) pyrite, (e) feldspar and (f) carbonate mineral content for core samples of the Wufeng-Longmaxi shale collected from three wells in the Anchang Syncline.
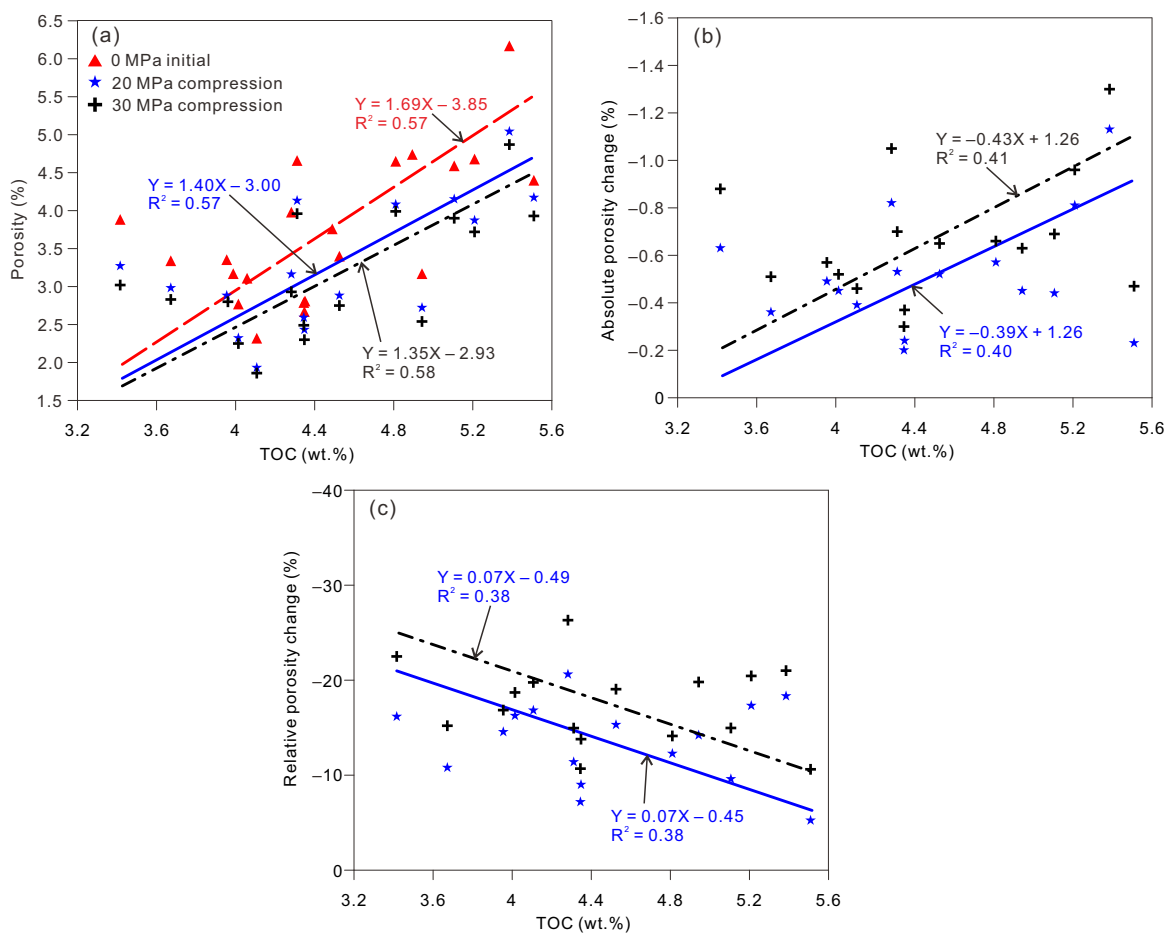
Fig. 6. Crossplots of TOC with (a) porosities measured before axial compression at 20 MPa compression and 30 MPa compression, (b) the absolute magnitude of porosity change (negative sign indicates porosity reduction) at compressions of 20 and 30 MPa and (c) the porosity change normalized with the initial porosity (i.e., before compression). All samples were collected from the Wufeng-Longmaxi shale of well A1.

porosity relationship (Loucks et al., 2012; Lohr et al., 2015). Primary pores associated with minerals or organic matter can be occluded by solid bitumen in the oil window, resulting in the lack of a strong interrelation between porosity and TOC (Loucks et al., 2012; Han et al., 2017). Nevertheless, solid bitumen can generate secondary pores at an elevated thermal maturity level during the transition from solid into aqueous or gaseous fluids. Vitrinite maceral sourced from the woody tissue of vascular plants barely appears in the Wufeng-Longmaxi shale (Hackley and Cardott, 2016). Nevertheless, bitumen reflectance and infrared spectroscopy analyses indicated that the Wufeng-Longmaxi shale in the Yangtze Block is generally highly matured to overmatured (Feng et al., 2018). A more direct estimation of thermal maturity level in the Wufeng-Longmaxi shale of the Anchang Syncline showed 1.92%-2.19% equivalent Ro (Zhai et al., 2017), which is too high to hold massive solid bitumen (Mastalerz et al., 2013; Han et al., 2017) and does not enable the effect of solid bitumen occlusion on the various TOC-porosity correlations (Fig. 5(a)). Curtis et al. (2012) pointed out that because of a variation in maceral types at the same thermal maturity level,

two organic particles in a single field of view can show a distinct difference in organic pore development. A comparative study on the pore generation potential between shales with various types of organic matter indicated that those dominated by type I generally have a potential that is 12 times stronger than that of type III-dominant shales (Chen et al., 2015). The kerogen in the Wufeng-Longmaxi shale in the Yangtze Block was predominantly type II and I. The slight variation in organic matter types may be attributed to changes in the deposition environment. The reported organic matter in the Wufeng-Longmaxi shale of the Anchang Syncline was type I, consisting primarily of amorphous macerals (Zhai et al., 2017). Moreover, mineral compositions, which are commonly used as a proxy for deposition, were almost uniform in the three wells of the Wufeng-Longmaxi shale (Fig. 3), suggesting a homogeneous sedimentary environment that led to a lack of lateral variation in the organic matter composition of the Anchang Syncline. Thus, there were no detectable variations in maceral type that could account for the differences in TOC-porosity correlations between the three wells.
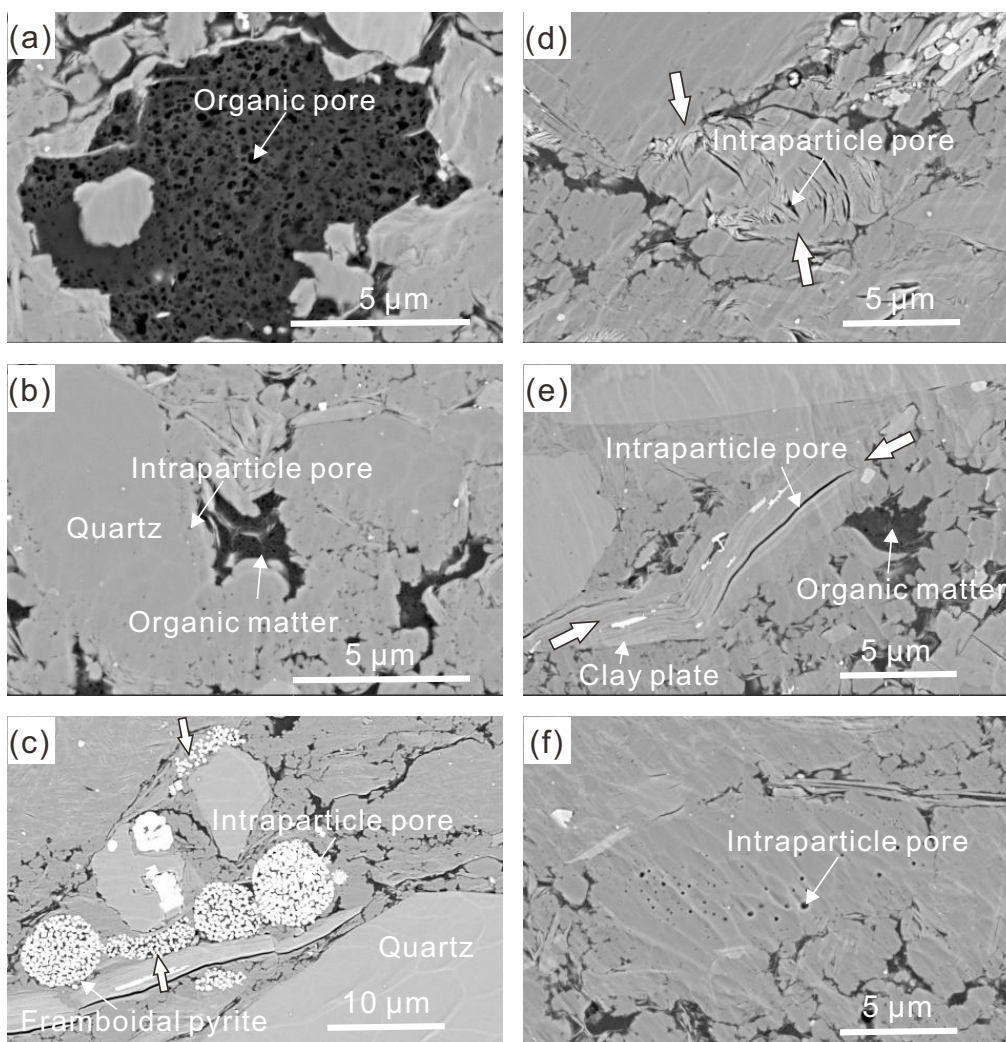
Fig. 7. FE-SEM observations of matrix components and pore structures in Wufeng-Longmaxi shale samples of the Anchang Syncline. (a) The amorphous organic matters with pores, at 1,972 m depth of well A2, (b) the amorphous organic matter and intraparticle pores, at 1,968 m depth of well A2, (c) framboidal pyrite with intraparticle pores, at 2,344 m of well A1; some of the framboidal pyrites were compressed in the orientation indicated by solid arrows, (d) intraparticle pores generated by stress compression in the orientation indicated by solid arrows, at 2,483 m of well A3, (e) the platy or flake-like clay with intraparticle pore, at 2,478 m depth of well A3, (f) intraparticle pores generated by dissolution in feldspar, at 2,334 m depth of well A1.

5.1.2 Oil expulsion efficiency

The secondary cracking of inefficiently expelled oil at an elevated thermal maturity level can generate post-oil bitumen that may migrate into open pore spaces and induce bitumen occlusion (Cardott et al., 2015; Pommer and Milliken, 2015; Liu et al., 2017b). Oil expulsion from matured shale is called primary migration in conventional petroleum systems, which is greatly promoted by fracture or fault systems. Basin modeling has suggested that the oil window of the Wufeng-Longmaxi shale in the Anchang Syncline appeared during the Permian and Triassic (Zhai et al., 2017) when regional deformation was driven by the collision between the North China Block and the Yangtze Block. During this collision, NNE-SSW-striking faults were widely formed in the Central Yangtze Block (Dong et al., 2020), including the Anchang Syncline (Fig. 9) (Lan et al., 2022). As shown in Fig. 9, wells A1, A2 and A3 were not cut by these NNE-SSW striking faults, implying the indistinctive variation in the oil expulsion between the three wells. Therefore, it can be concluded that oil expulsion was not responsible for variations in the relationship between porosity and TOC content in the Wufeng-Longmaxi shale of the Anchang Syncline.

5.1.3 Mineral diagenesis

The absence of a clear relationship between bulk porosity and TOC content may indicate the presence of massive pore formation or destruction caused by mineral diagenesis (Milliken et al., 2012). In the Barney Creek Formation of McArthur
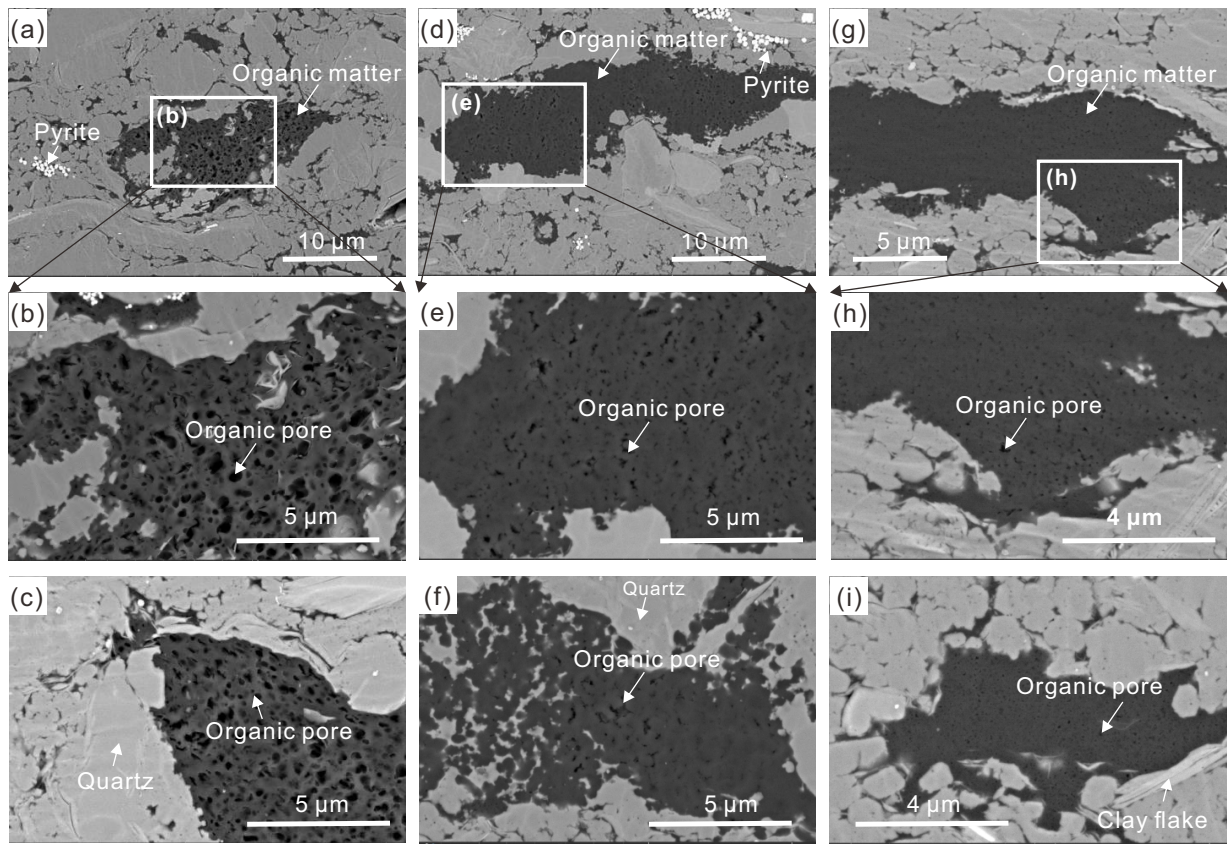
Fig. 8. FE-SEM observations of organic pore size, shape, and alignment changes in the Wufeng-Longmaxi shale samples collected from (a-c) well A2, (d-f) well A1 and (g-i) well A3 in the Anchang Syncline.
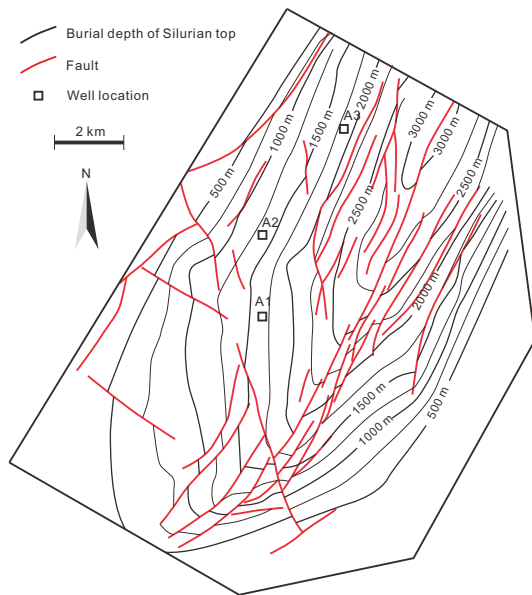
Fig. 9. Fault system cutting the Wufeng-Longmaxi shale in the Anchang Syncline (Lan et al., 2022).

Basin, Australia, precipitations of clays and submicron quartz caused the absence of organic pores during the transition from thermally immature to mature stages; subsequently, secondary pores were produced by the dissolution of carbonates and feldspar by organic acids under a high thermal maturity-enhanced porosity (Baruch et al., 2015). Mineral-associated pores controlled by deposition and diagenesis processes (e.g., interparticle and intraparticle pores) were indeed identified in the FE-SEM observation of the Wufeng-Longmaxi shale in the Anchang Syncline (Figs. 7(b)-7(f)). There was no detectable variation in the mineral compositions of the three wells (Fig. 3), which implied the absence of lateral variation in the deposition. Nevertheless, the complicated correlations between porosity and mineral content suggested a spatial difference in the chemically or mechanically powered diagenesis processes (Figs. 5(b)-5(d)).

Porosity correlated negatively and positively with clay the content of samples from wells A2 and A3, respectively (Fig. 5(b)). The precipitation of clay in pore spaces reduced the porosity and reasonably accounted for the negative porosity-clay correlation (Baruch et al., 2015). In contrast, slipping between clay flakes under intensive effective stress generated pore spaces (Zhu et al., 2018) (Fig. 7(e)), which may have resulted in the positive porosity-clay correlation in samples obtained from well A3.

Positive and negative correlations between porosity and quartz content appeared in the samples of wells A2 and A3, respectively (Fig. 5(c)). The resistance of effective stress by
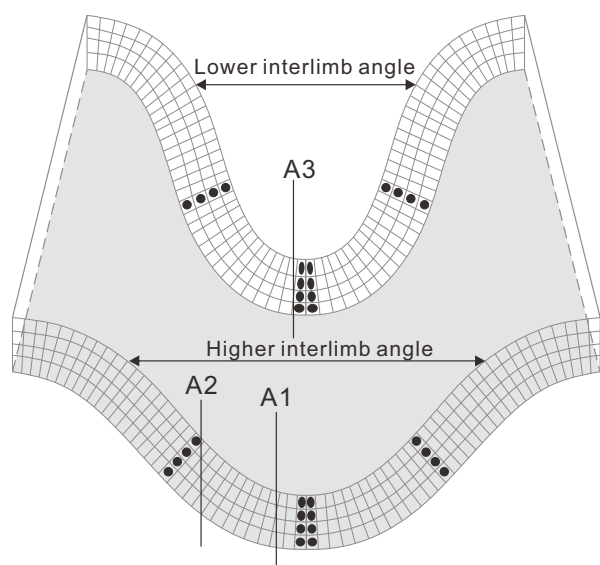
Fig. 10. Illustration of spatial change in organic pores in the Wufeng-Longmaxi shale with structural domains in the Anchang Syncline.

the framework of rigid-matrix minerals (e.g., quartz or pyrite) inhibited the compaction of pores and resulted in a positive porosity-quartz correlation (Dong et al., 2019; Knapp et al., 2020). Thus, a positive porosity-pyrite correlation was generally identified in the Wufeng-Longmaxi shale samples from the Anchang Syncline (Fig. 5(d)). It seems that the protection of pore spaces by rigid pyrites was relatively weaker in samples obtained from wells A1 and A3, which was potentially related to the failure of resistance, as indicated by the flattening of some framboidal pyrite at the stress concentration points (Fig. 7(c)). Similarly, the stress resistance of quartz grains failed to maintain a positive porosity-quartz correlation in samples obtained from wells A1 and A3 (Fig. 5(c)). Notably, a negative porosity-quartz correlation was present in samples from well A3, which may be a residual sign of the precipitation of submicron quartz in pore spaces (Baruch et al., 2015).

Despite the appearance of dissolution pores in the FE-SEM images (Fig. 7(f)), there was no clear correlation between porosity and the presence of relatively soluble minerals (e.g., feldspar and carbonates) (Figs. 5(e) and 5(f)), implying the vital influence of mineral dissolution on the porosity of Wufeng-Longmaxi shale of the Anchang Syncline.

5.1.4 Structural compaction

The destruction of organic pores during structural deformation was reported to obscure the TOC-porosity correlation in the organic-rich shale of fold-thrust belts (Milliken et al., 2013; Liu et al., 2020a, 2020b). Organic matter, particularly amorphous macerals, are much more compressible relative to mineral matrices under equivalent stress or temperature conditions (Eliyahu et al., 2015). Thus, the lack of organic pores and the poor TOC-porosity relationship in the early oil window were also suspected to be caused by the compaction of elevated vertical effective stress (overburden stress) (Curtis et al., 2012; Lohr et al., 2015; Wang, 2020). Nevertheless, the

overpressure originating from organic matter or oil cracking at elevated thermal maturity was suggested to restrain the elevation of vertical effective stress or even result in the unloading of vertical effective stress (Tingay et al., 2013). Thus, it seems that organic pores generated after the oil window were barely compacted during the monotonic burial process and commonly show spherical shapes inherited from the nucleation of gas bubbles from liquid oil or viscous bitumen (Milliken et al., 2013; Schieber, 2010, 2013). However, the thermally induced overpressure generally failed to resist the horizontal tectonic stress under the compression settings. Except for the inherited biological structure (Lohr et al., 2015), changes in the size, shape, and alignment of organic pores were commonly recognized in the organic shale of tectonic compression settings (Milliken et al., 2013; Liu et al., 2020a, 2020b; Wang, 2020). For instance, pore morphology and alignments were altered by evolving a higher aspect ratio and developing increasingly perpendicular to the compression orientation. Porosity became abnormally low at an elevated TOC content or even independent of the TOC content.

As mentioned in Section 5.1.3, mechanical diagenesis (i.e., compaction powered by effective stress) altered the porosity of Wufeng-Longmaxi shale in the Anchang Syncline. Relative to well A2, samples in wells A1 and A3, which were located closer to the syncline hinge zone and generally suffered more intensive tectonic deformation strain, exhibited lower porosity under a similar content of rigid matrix minerals (Figs. 5(c) and 5(d)). Even relative to well A1, a decrease in porosity in samples obtained from well A3, which had a lower interlimb angle, was also found. Overwhelmingly, organic pores with diameters of > 50 nm commonly showed spherical shapes in the samples of well A2 (Figs. 8(a)-8(c)), whereas organic pores prevailed in a smaller size (2-50 nm diameter) and showed polygonal, elongate and slit morphologies in the samples of wells A1 and A3 (Figs. 8(d)-8(i)). The decrease in pore size and increase in aspect ratio also suggested the compaction and collapse of organic pores in the Wufeng-Longmaxi shale in the hinge zone of Anchang Syncline during tectonic compression (Figs. 10 and 11). Therefore, it seems that spatial variation in the structural deformation strain contributed to the difference in TOC-porosity correlation in the Wufeng-Longmaxi shale of the Anchang Syncline.

In order to further verify the influence of structural deformation or compaction, samples of the Wufeng-Longmaxi shale obtained from well A1 were artificially compacted to parallel the deposition beddings. As shown in Fig. 6(a), more intensive compaction generally induced a greater porosity decrease at a similar TOC content. Meanwhile, a higher content of ductile organic matter seemed to result in a stronger structural compaction under similar compression stress, as indicated by a large change in porosity (Fig. 6(b)).

5.2 Implications for shale gas exploration in the fold-thrust belt

The fold-thrust belt of the Yangtze Block was mainly created by regional compression driven by the subduction of the Cathaysian Block and the uplift of the Jiangnan-Xuefeng
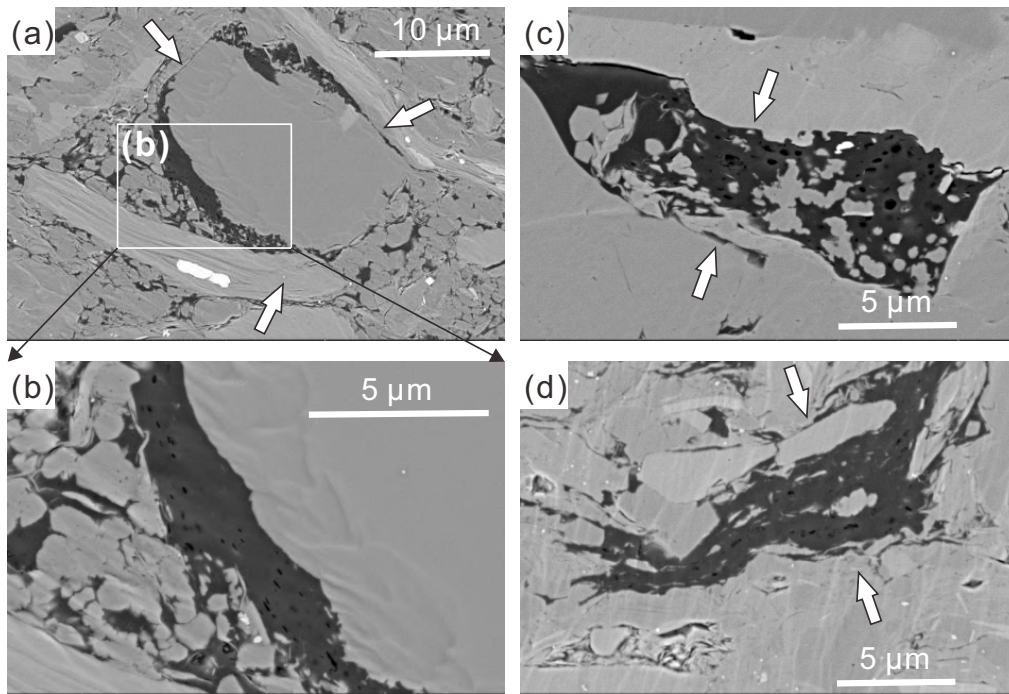
Fig. 11. FE-SEM observations showing the organic pore deformation in the Wufeng-Longmaxi shale of well A1 in the Anchang Syncline. (a) and (b) the residual organic pores in the pressure shadow of quartz and clay flakes, at depth of 2,340 m. Deformation of organic pores (c) at depth of 2,338 m and (d) at depth of 2,341 m. The alignment of organic pores was controlled by stress compression in the orientation indicated by solid arrows.
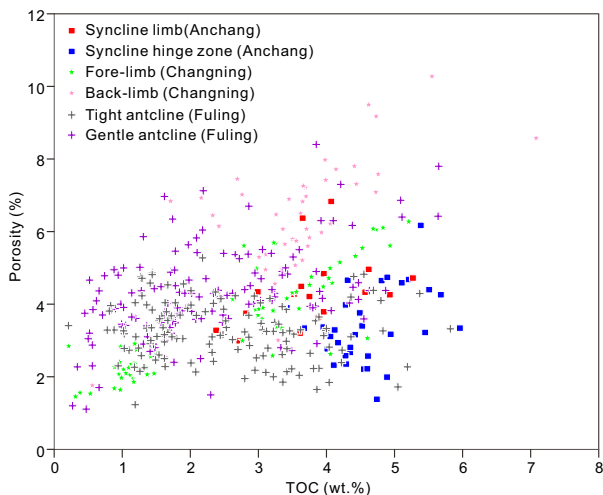
Fig. 12. A regional comparison of TOC-porosity correlation in the Yangtze Block. Data on the Changning and Fuling gas fields were adapted from Liu et al. (2020a, 2020b), respectively.

Orogen (Fig. 1(a)). The distance to the Jiangnan-Xufeng Orogen generally increases from the Anchang Syncline to the Fuling and Changning areas. By integrating the data of Anchang Syncline, Fuling area and Changning area, the general effect of tectonism on pores in the Wufeng-Longmaxi shale in the fold-thrust belt of Yangtze Block was revealed, as shown in Fig. 11.

Regionally, the Wufeng-Longmaxi shale of the Anchang

Syncline that is spatially located closer to the Jiangnan-Xufeng Orogen (Fig. 1(a)) suffered more intensive tectonic compaction of shale porosity relative to that of the Changning area at a constant TOC content. Despite the influences of engineering specifications (e.g., horizontal well numbers, horizontal length, and fracturing stages) on the daily production, the Wufeng-Longmaxi shale in the Anchang Syncline recently yielded a tested daily production of approximately 7×10^4 m^3 (an average of 3×10^4 m^3) per well, which is almost half of the tested daily production of approximately 14×10^4 m^3 obtained from the first commercial shale gas well in the Changning area during 2010. Shale pores, as the potential migration pathways and principal storage room for gas molecules in organic-rich shales, seem to directly control the gas resource potential and difficulty of recovery in the fold-thrust belt.

Data on the Wufeng-Longmaxi shale in the Fuling gas field, which was the first commercial shale gas field outside North America (Delle Piane et al., 2021) and is spatially located between the Anchang Syncline and Changning field, show two distinct tendencies in the gentle and tight anticlines in terms of the degree of tectonic compaction (Liu et al., 2020a) (Fig. 11).

We found that the tendencies in the gentle and tight anticlines aligned with the data of the Changning area and Anchang Syncline, respectively (Fig. 12). One of the tight anticlines in the Fuling field, called the Pingqiao Anticline, yielded a tested daily production as high as 89.5×10^4 m^3 (an average of 21.99×10^4 m^3) from the Wufeng-Longmaxi shale, with an average TOC content of 3.42 wt.% (with a range of

1.81 to 5.98 wt.%) and an average porosity of 3.23% (with a range of 1.06% to 4.62%) (Guo, 2019). Despite the tectonic compaction of shale pores, the high density of brittle fractures preserved massive amounts of methane and resulted in a high daily production from the Wufeng-Longmaxi shale of the tight Pingqiao Anticline (Xu et al., 2019). Therefore, the Wufeng-Longmaxi shale, which is rich in fractures between the roof and floor layers, may continue to be an excellent exploration target in the fold-thrust belt of the Yangtze Block, including the Anchang Syncline.

6. Conclusions

In this study, we performed a systematic comparative investigation, involving organic or inorganic matrix composition, petrography, bulk porosity, and artificial axial compression experiments in the Wufeng-Longmaxi shale of the Anchang Syncline in the fold-thrust belt of the Central Yangtze Block, to reveal the structural deformation of organic-rich shales during exhumation.

The porosity of Wufeng-Longmaxi shale was generally positively correlated with the TOC content in the Anchang Syncline. Despite the same TOC content, shale porosity was commonly reduced in wells moving from the syncline limb to the syncline hinge zone, and it also dropped with decreasing interlimb angles in the wells located in the syncline hinge zone. These spatial changes in the porosity of Wufeng-Longmaxi shale are generally aligned with the structural deformation strain during folding. Artificial axial compression tests of Wufeng-Longmaxi shale of the Anchang Syncline confirmed the distinct decrease in shale porosity after compression. The absolute magnitude of this porosity change was positively correlated with axial compression stress and was generally higher in samples with a higher TOC content. The organic pore size decreased, whereas the aspect ratio of the pore shape increased with an increase in structural deformation strain. The resistance of effective stress by quartz seemed to fail under intensive structural deformation strain, thereby changing the relationship between porosity and quartz from positive to negative. In contrast, the slipping between clay flakes under intensive effective stress generated pore spaces, which resulted in a positive relationship between clay mineral content and porosity.

As compared with commercial shale gas fields in the Sichuan Basin, the Anchang Syncline is spatially closer to the collision boundary between the Yangtze and Cathaysian blocks, and also suffered an intensive tectonic deformation of shale pores. Although this phenomenon generally decreased the shale porosity, shales rich in microfractures may remain excellent exploration targets in the fold-thrust belt of the Yangtze Block, including the Anchang Syncline.

Acknowledgement

Conflict of interest

The authors declare no competing interest.

References

Athy, L. F. Density, porosity, and compaction of sedimentary rocks. AAPG Bulletin, 1930, 14(1): 1-24.

Baruch, E. T., Kennedy, M. J., Löhr, S. C., et al. Feldspar dissolution-enhanced porosity in Paleoproterozoic shale reservoir facies from the Barney Creek Formation (McArthur Basin, Australia). AAPG Bulletin, 2015, 99(9): 1745-1770.

Bernard, S., Horsfield, B., Schulz, H. M., et al. Geochemical evolution of organic-rich shales with increasing maturity: A STXM and TEM study of the Posidonia shale (Lower Toarcian, northern Germany). Marine and Petroleum Geology, 2012a, 31(1): 70-89.

Bernard, S., Wirth, R., Schreiber, A., et al. Formation of nanoporous pyrobitumen residues during maturation of the Barnett shale (Fort Worth Basin). International Journal of Coal Geology, 2012b, 103: 3-11.

Bjørlykke, K. Relationships between depositional environments, burial history and rock properties. Some principal aspects of diagenetic process in sedimentary basins. Sedimentary Geology, 2014, 301: 1-14.

Cai, J., Zhao, L., Zhang, F., et al. Advances in multiscale rock physics for unconventional reservoirs. Advances in Geo-Energy Research, 2022, 6(4): 271-275.

Cardott, B. J., Landis, C. R., Curtis, M. E. Post-oil solid bitumen network in the Woodford shale, USA—A potential primary migration pathway. International Journal of Coal Geology, 2015, 139: 106-113.

Chalmers, G. R. L., Bustin, R. M. The organic matter distribution and methane capacity of the Lower Cretaceous strata of Northeastern British Columbia, Canada. International Journal of Coal Geology, 2007, 70(1): 223-239.

Chen, Z., Wang, T., Liu, Q., et al. Quantitative evaluation of potential organic-matter porosity and hydrocarbon generation and expulsion from mudstone in continental lake basins: A case study of Dongying sag, eastern China. Marine and Petroleum Geology, 2015, 66: 906-924.

Chen, S., Yao, S., Wang, Y., et al. Investigation of pore evolution and variation with magma intrusion on Permian Gufeng shale formation and their implications on gas enrichment. Journal of Natural Gas Science and Engineering, 2021, 96: 104277.

Curtis, M. E., Ambrose, R. J., Sondergeld, C. H. Structural characterization of gas shales on the micro- and nano-scales. Paper SPE 137693 Presented at the Canadian Unconventional Resources and International Petroleum Conference, Calgary, Alberta, Canada, 19-21 October, 2010.

Curtis, M. E., Cardott, B. J., Sondergeld, C. H., et al. Development of organic porosity in the Woodford shale with

increasing thermal maturity. International Journal of Coal Geology, 2012, 103: 26-31.

Delle Piane, C., Ansari, H., Li, Z., et al. Influence of organic matter type on porosity development in the Wufeng-Longmaxi shale: A combined microscopy, neutron scattering and physisorption approach. International Journal of Coal Geology, 2022, 249: 103880.

Dong, T., He, S., Chen, M., et al. Quartz types and origins in the paleozoic Wufeng-Longmaxi Formations, Eastern Sichuan Basin, China: Implications for porosity preservation in shale reservoirs. Marine and Petroleum Geology, 2019, 106: 62-73.

Dong, S., Li, J., Cawood, P. A., et al. Mantle influx compensates crustal thinning beneath the Cathaysia Block, South China: Evidence from SINOPROBE reflection profiling. Earth Planet. Earth and Planetary Science Letters, 2020, 544: 116360.

Dong, S., Zhang, Y., Gao, R., et al. A possible buried Paleoproterozoic collisional orogen beneath central South China: Evidence from seismic-reflection profiling. Precambrian Research, 2015, 264: 1-10.

Eliyahu, M., Emmanuel, S., Day-Stirrat, R. J., et al. Mechanical properties of organic matter in shales mapped at the nanometer scale. Marine and Petroleum Geology, 2015, 59: 294-304.

Evans, K. F., Oertel, G., Engelder, T. Appalachian Stress Study: 2. Analysis of Devonian shale core: Some implications for the nature of contemporary stress variations and Alleghanian deformation in Devonian rocks. Journal of Geophysical Research: Solid Earth, 1989, 94(B6): 7155-7170.

Feng, W., Wang, F., Guan, J., et al. Geologic structure controls on initial productions of lower Silurian Longmaxi shale in south China. Marine and Petroleum Geology, 2018, 91: 163-178.

Fishman, N. S., Hackley, P. C., Lowers, H. A., et al. The nature of porosity in organic-rich mudstones of the Upper Jurassic Kimmeridge Clay Formation, North Sea, offshore United Kingdom. International Journal of Coal Geology, 2012, 103: 32-50.

Fraser-Harris, A., Lightbody, A., Edlmann, K., et al. Sampling and preparation of c.200 mm diameter cylindrical rock samples for geomechanical experiments. International Journal of Rock Mechanics and Mining Sciences, 2020, 128: 104233.

Gao, Z., Fan, Y., Xuan, Q., et al. A review of shale pore structure evolution characteristics with increasing thermal maturities. Advances in Geo-Energy Research, 2020, 4(3): 247-259.

Gou, Q., Xu, S., Hao, F., et al. The effect of tectonic deformation and preservation condition on the shale pore structure using adsorption-based textural quantification and 3D image observation. Energy, 2021, 219: 119579.

Gu, Y., He, J., Xu, S., et al. Influence of differential structural deformation on shale reservoirs: a case study of the lower Silurian Longmaxi shale in north Guizhou, Southern China. Geological Magazine, 2021, 158(4): 673-684.

Guo, X. Controlling factors on shale gas accumulations of

Wufeng-Longmaxi Formations in Pingqiao shale gas field in Fuling area, Sichuan Basin. Natural Gas Geoscience, 2019, 30(1): 1-10. (in Chinese)

Hackley, P. C., Cardott, B. J. Application of organic petrography in North American shale petroleum systems: A review. International Journal of Coal Geology, 2016, 163: 8-51.

Han, Y., Horsfield, B., Wirth, R., et al. Oil retention and porosity evolution in organic-rich shales. AAPG Bulletin, 2017, 101(6): 807-827.

Hao, F., Zou, H. Cause of shale gas geochemical anomalies and mechanisms for gas enrichment and depletion in high-maturity shales. Marine and Petroleum Geology, 2013, 44: 1-12.

Hou, Y., Gao, J., Ren, K., et al. Variations of lacustrine shale reservoirs in different deformation zones of Mohe Basin, northeastern China: Insights into the impact of thrust nappe structure on shale gas preservation. Marine and Petroleum Geology, 2021, 133: 105272.

Hu, H., Zhang, T., Wiggins-Camacho, J. D., et al. Experimental investigation of changes in methane adsorption of bitumen-free Woodford shale with thermal maturation induced by hydrous pyrolysis. Marine and Petroleum Geology, 2015, 59: 114-128.

Javie, D. M. Shale resource systems for oil and gas: part I—shale gas resource systems. Part II—shale oil resource systems. Shale reservoirs-giant resources for the 21st century. AAPG Memoir, 2012, 97: 69-87.

Katz, B. J., Arango, I. Organic porosity: A geochemist's view of the current state of understanding. Organic Geochemistry, 2018, 123: 1-16.

Klaver, J., Desbois, G., Littke, R., et al. BIB-SEM characterization of pore space morphology and distribution in postmature to overmature samples from the Haynesville and Bossier shales. Marine and Petroleum Geology, 2015, 59: 451-466.

Knapp, L. J., Ardakani, O. H., Uchida, S., et al. The influence of rigid matrix minerals on organic porosity and pore size in shale reservoirs: Upper Devonian Duvernay Formation, Alberta, Canada. International Journal of Coal Geology, 2020, 227: 103525.

Ko, L. T., Loucks, R. G., Zhang, T., et al. Pore and pore network evolution of Upper Cretaceous Boquillas (Eagle Ford-equivalent) mudrocks: Results from gold tube pyrolysis experiments. AAPG Bulletin, 2016, 100(11): 1693-1722.

Ko, L. T., Ruppel, S. C., Loucks, R. G., et al. Pore-types and pore-network evolution in Upper Devonian-Lower Mississippian Woodford and Mississippian Barnett mudstones: Insights from laboratory thermal maturation and organic petrology. International Journal of Coal Geology, 2018, 190: 3-28.

Lan, B., Zhao, F., Li, S., et al. Investigation of the enrichment and accumulation of normal pressure shale gas in Anchang syncline outside of Sichuan Basin. Frontiers in Earth Science, 2022, 9: 802142.

Li, K., Kong, S., Xia, P., et al. Microstructural characterisation of organic matter pores in coal-measure shale. Advances

in Geo-Energy Research, 2020, 4(4): 372-391.

Liu, R., Hao, F., Engelder, T., et al. Stress memory extracted from shale in the vicinity of a fault zone: Implications for shale-gas retention. Marine and Petroleum Geology, 2019, 102(4): 340-349.

Liu, R., Hao, F., Engelder, T., et al. Influence of tectonic exhumation on porosity of Wufeng-Longmaxi shale in the Fuling gas field of the eastern Sichuan Basin, China. AAPG Bulletin, 2020a, 104(4): 939-959.

Liu, B., Schieber, J., Mastalerz, M. Combined SEM and reflected light petrography of organic matter in the New Albany shale (Devonian-Mississippian) in the Illinois Basin: A perspective on organic pore development with thermal maturation. International Journal of Coal Geology, 2017a, 184: 57-72.

Liu, Y., Xiong, Y., Li, Y., et al. Effects of oil expulsion and pressure on nanopore development in highly mature shale: Evidence from a pyrolysis study of the Eocene Maoming oil shale, south China. Marine and Petroleum Geology, 2017b, 86: 526-536.

Liu, R., Zheng, J., Hao, F., et al. Variation in pore systems with tectonic stress in the overthrust Wufeng-Longmaxi shale of the southern Sichuan Basin, China. Journal of Natural Gas Science and Engineering, 2020b, 83: 103617.

Löhr, S. C., Baruch, E. T., Hall, P. A., et al. Is organic pore development in gas shales influenced by the primary porosity and structure of thermally immature organic matter? Organic Geochemistry, 2015, 87: 119-132.

Loucks, R. G., Reed, R. M., Ruppel, S. C., et al. Morphology, genesis, and distribution of nanometer-scale pores in siliceous mudstones of the Mississippian Barnett shale. Journal of Sedimentary Research, 2009, 79(12): 848-861.

Loucks, R. G., Reed, R. M., Ruppel, S. C., et al. Spectrum of pore types and networks in mudrocks and a descriptive classification for matrix-related mudrock pores. AAPG Bulletin, 2012, 96(6): 1071-1098.

Ma, Y., Ardakani, O. H., Zhong, N., et al. Possible pore structure deformation effects on the shale gas enrichment: An example from the Lower Cambrian shales of the Eastern Upper Yangtze Platform, South China. International Journal of Coal Geology, 2020, 217: 103349.

Mastalerz, M., Schimmelmann, A., Drobniak, A., et al. Porosity of Devonian and Mississippian New Albany shale across a maturation gradient: Insights from organic petrology, gas adsorption, and mercury intrusion. AAPG Bulletin, 2013, 97(10): 1621-1643.

Mathia, E. J., Bowen, L., Thomas, K. M., et al. Evolution of porosity and pore types in organic-rich, calcareous, Lower Toarcian Posidonia shale. Marine and Petroleum Geology, 2016, 75: 117-139.

McGlade, C., Speirs, J., Sorrell, S. Unconventional gas-A review of regional and global resource estimates. Energy, 2013, 55: 571-584.

Melchin, M. J., Mitchell, C. E., Holmden, C., et al. Environmental changes in the Late Ordovician-early Silurian: Review and new insights from black shales and nitrogen isotopes. GSA Bulletin, 2013, 125(11-12): 1635-1670.

Milliken, K. L., Esch, W. L., Reed, R. M., et al. Grain assemblages and strong diagenetic overprinting in siliceous mudrocks, Barnett shale (Mississippian), Fort Worth Basin, Texas. AAPG Bulletin, 2012, 96(8): 1553-1578.

Milliken, K. L., Rudnicki, M., Awwiller, D. N., et al. Organic matter-hosted pore system, Marcellus Formation (Devonian), Pennsylvania. AAPG Bulletin, 2013, 97(2): 177-200.

Pommer, M., Milliken, K. Pore types and pore-size distributions across thermal maturity, Eagle Ford Formation, southern Texas. AAPG Bulletin, 2015, 99(9): 1713-1744.

Schieber, J. Common themes in the formation and preservation of intrinsic porosity in shales and mudstones-illustrated with examples across the Phanerozoic. Paper SPE 132370 Presented at SPE Unconventional Gas Conference, Pittsburgh, Pennsylvania, 23-25 February, 2010.

Schieber, J. Observations on ion-milled samples of Devonian Black Shales from Indiana and New York: The petrographic context of multiple pore types. AAPG Memoir 102, 2013: 153-171.

Screaton, E., Saffer, D., Henry, P., et al. Porosity loss within the underthrust sediments of the Nankai accretionary complex: Implications for overpressures. Geology, 2002, 30(1): 19-22.

Sheng, G., Su, Y., Zhao, H., et al. A unified apparent porosity/permeability model of organic porous media: Coupling complex pore structure and multi-migration mechanism. Advances in Geo-Energy Research, 2020, 4(2): 115-125.

Shi, S., Wang, Y., Guo, H., et al. Variations in pore structure of marine shale from the same horizon of the Longmaxi Formation with changing position in a small-scale anticline: Implications for the influence of structural deformation. Marine and Petroleum Geology, 2021, 124: 104837.

Sun, L., Tuo, J., Zhang, M., et al. Formation and development of the pore structure in Chang 7 member oil-shale from Ordos Basin during organic matter evolution induced by hydrous pyrolysis. Fuel, 2015, 158: 549-557.

Tingay, M. R. P., Morley, C. K., Laird, A., et al. Evidence for overpressure generation by kerogen-to-gas maturation in the northern Malay Basin. AAPG Bulletin, 2013, 97(4): 639-672.

Wang, G. Deformation of organic matter and its effect on pores in mud rocks. AAPG Bulletin, 2020, 104(1): 21-36.

Xiang, J., Zhu, Y., Wang, Y., et al. Structural deformation and its pore-fracture system response of the Wufeng-Longmaxi shale in the Northeast Chongqing area, using FE-SEM, gas adsorption, and SAXS. Journal of Petroleum Science and Engineering, 2021, 209: 109877.

Xu, S., Gou, Q., Hao, F., Zhang, B., et al. Shale pore structure characteristics of the high and low productivity wells, Jiaoshiba Shale Gas Field, Sichuan Basin, China: Dominated by lithofacies or preservation condition? Marine and Petroleum Geology, 2020, 114: 104211.

Xu, S., Liu, R., Hao, F., et al. Complex rotation of maximum horizontal stress in the Wufeng-Longmaxi shale on the eastern margin of the Sichuan Basin, China: Implications for predicting natural fractures. Marine and Petroleum Geology, 2019, 109(11): 519-529.

Zhai, G., Bao, S., Pang, F., et al. Peservoir-forming pattern of "four-storey" hydrocarbon accumulation in Anchang syncline of northern Guizhou Province. Geology in China, 2017, 44(1): 1-12. (in Chinese)

Zhang, F., Huang, Y., Lan, B., et al. Characteristics and controlling factors of shale reservoir in Wufeng Formation-Longmaxi Formation of the Zheng'an area. Bulletin of Geological Science and Technology, 2021, 40(1): 49-56. (in Chinese)

Zhu, H., Ju, Y., Huang, C., et al. Pore structure variations across structural deformation of Silurian Longmaxi shale: An example from the Chuandong Thrust-Fold Belt. Fuel, 2019, 241: 914-932.

Zhu, H., Ju, Y., Qi, Y., et al. Impact of tectonism on pore type and pore structure evolution in organic-rich shale: Implications for gas storage and migration pathways in naturally deformed rocks. Fuel, 2018, 228: 272-289.

Zou, C., Qiu, Z., Poulton, S. W., et al. Ocean euxinia and climate change "double whammy" drove the Late Ordovician mass extinction. Geology, 2018, 46(6): 535-538.